JOURNAL OF PROPULSION AND POWER
Vol. 16, No. 5, September–October 2000

Unsteady Blade-Row Flow Calculations Using a Low-Reynolds-Number Turbulence Model

Chang Ho Choi* and Jung Yul Yoo†
Seoul National University, Seoul 151-742, Republic of Korea

A computational study on unsteady compressible flows has been performed by adopting a low-Reynolds-number k–ω turbulence model in conjunction with dual-time-stepping and multigrid schemes. An explicit four-stage Runge–Kutta scheme for the Navier–Stokes equations and an approximate factorization scheme for the k–ω turbulence model equations are adopted for dual-time stepping. Computational results for unsteady shock-wave boundary-layer interaction in the case of shock buffeting phenomena around a bicircular-arc airfoil are in good agreement with extant experimental data, as well as those for blade surface-pressure distributions in the case of rotor-stator interaction in a turbine stage. Comparisons of the results obtained by the k–ω and algebraic turbulence models indicate that the effect of turbulence models on the surface-pressure distributions is not so significant in the case of rotor-stator interaction as in the case of shock buffeting phenomena, which depend on the extent of the separated region involved. However, based on the results obtained by the k–ω model, the effects of the wake from the stator on the boundary-layer transition over the rotor blade surface can be explained by showing that high-intensity turbulence of the stator wake induces an early transition.

Introduction

MODERN turbomachinery requires increased durability, high performance, and reduced noise levels in a smaller size and with fewer components. To achieve these design criteria, an accurate understanding of the effects of flow unsteadiness is essential because turbomachinery flows are basically unsteady because of interactions between adjacent blade rows. There are three types of such interactions, which are called potential-flow, wake, and shock-wave interactions.[1] These interactions are known to cause unsteady aerodynamic excitations that can induce blade vibrations, generate discrete-tone noise, and degrade aerodynamic efficiency.[2]

Four categories of numerical procedures for analyzing flows in multistage turbomachinery can be made according to how the boundary conditions are prescribed at a common grid interface between adjacent blade rows[1,3]: 1) steady single blade-row techniques,[4] 2) steady coupled blade-row techniques,[3] 3) loosely coupled blade-row techniques (LCBR),[1,2] and 4) unsteady fully coupled techniques.[5–12] Among them, only unsteady fully coupled simulation solves the flowfield of multiple blade rows simultaneously without any modeling except for turbulence. Therefore, this approach requires enormous computer resources. But all of the important physics of unsteady interaction can be accurately preserved within the limits of turbulence modeling. This fully unsteady method was first used by Rai,[5,6] who solved two-dimensional and three-dimensional thin-layer Navier–Stokes equations using a system of patched and overlaid grids for a rotor/stator configuration of an axial turbine in conjunction with an iterative, factored, implicit algorithm. Then, Madavan et al.[7] developed and validated a three-dimensional multipassage Navier–Stokes code for predicting the unsteady effects caused by turbine rotor-stator interaction. Arnone et al.[8] proposed a dual-time stepping method to solve a rotor-stator interaction in conjunction with a multigrid scheme.

Whereas the preceding authors adopted algebraic turbulence models, more efforts are being focused on the use of two-equation turbulence models. Dorney[9] and Dorney and Ashpis[10] used a viscous unsteady quasi-three-dimensional Navier–Stokes analysis to quantify the Reynolds-number dependence of low-pressure turbine cascades and stages by adopting the k–ϵ model. Hah et al.[11] developed a three-dimensional, unsteady, viscous aerodynamic analysis for the flow inside a transonic, high-through-flow, single-stage compressor, applying a two-equation low-Reynolds-number turbulence model of Chien.[13] Very recently, Dorney et al.[12] used an unsteady quasi-three-dimensional Navier–Stokes analysis to investigate the unsteady aerodynamics of stator clocking in a one-and-one-half stage compressor.

The present study has been performed in line with this trend by adopting a low-Reynolds-number two-equation turbulence model in the hope that it can simulate better the convection of turbulence in the process of rotor-stator interaction than the algebraic turbulence model. Among the two-equation turbulence models, the k–ω model suggested by Wilcox[14] and modified by Menter[15] has the advantages that it does not require damping functions in the viscous sublayer and that the model equations are mathematically simpler and less stiff near the wall. Furthermore, it has been designed to achieve more accurate predictions for adverse-pressure-gradient flows. These features offered by the k–ω model have motivated the present applications.

Thus, the objective of the present study is to examine the unsteady aerodynamic phenomena by adopting a low-Reynolds-number k–ω model in comparison with the algebraic turbulence model. The applicability of the k–ω model to the unsteady separating and wake flow problems is examined by considering the unsteady shock buffeting phenomena over a bicircular-arc airfoil, where the shock waves oscillate and shock-induced separations occur. This problem is chosen because of its well-documented experimental results[16–18] and similarity to turbomachinery blade-row flows. Then, fully unsteady and steady averaging-plane approaches for analyzing the turbine rotor-stator interaction are applied to study blade surface-pressure distributions by comparing with available experimental data and to consider the effects of the wake from the stator on the boundary-layer transition over the rotor blade surface.

Numerical Method

Governing Equations

The system of governing equations considered in the present study consists of the time-dependent two-dimensional Reynolds-averaged Navier–Stokes equations and low-Reynolds-number k–ω model equations, which can be written in a conservative form as follows:

$$\frac{\partial Q}{\partial t} = -\left(\frac{\partial E_c}{\partial x} + \frac{\partial F_c}{\partial y}\right) + \left(\frac{\partial E_v}{\partial x} + \frac{\partial F_v}{\partial y}\right) + S = R(Q) \quad (1)$$

Received 19 October 1998; revision received 23 September 1999; accepted for publication 23 September 1999.

*Ph.D. Student, School of Mechanical and Aerospace Engineering.
†Professor, School of Mechanical and Aerospace Engineering. Member AIAA.

where $Q = [\rho, \rho u, \rho v, \rho E, \rho k, \rho\omega]^T$, the vectors E_c and F_c account for the convective terms, E_v and F_v the viscous terms, and S the source terms. More specifically, the source terms are present only in the turbulence model equations and can be defined as

$$S = J^{-1}\begin{bmatrix} \tau_{ij}\dfrac{\partial u_i}{\partial x_j} - \beta^*\rho\omega k \\ \left(\dfrac{\alpha\omega}{k}\right)\tau_{ij}\dfrac{\partial u_i}{\partial x_j} - \beta\rho\omega^2 + \sigma_d \end{bmatrix} \tag{2}$$

where the closure coefficients α, β, β^* are chosen in accordance with Wilcox[14] and the last term σ_d is included to remove the sensitivity of the k–ω model to the freestream value of ω such that

$$\sigma_d = \sigma\frac{\rho}{\omega}\max\left\{0, \frac{\partial k}{\partial x_j}\frac{\partial \omega}{\partial x_j}\right\} \tag{3}$$

according to Menter.[15]

Time-Stepping Scheme

Navier–Stokes Equations

As shown by Jameson[19] and Arnone et al.,[20] the Navier–Stokes equations written in the form of Eq. (1) can be reformulated in such a way that a time-marching steady-state solver can be applied to them. That is, by introducing a fictitious time τ, Eq. (1) can be reformulated with a new residual R^* as follows:

$$\frac{\partial Q}{\partial \tau} = \frac{\partial Q}{\partial t} - R(Q) = R^*(Q) \tag{4}$$

To reduce the new residual R^*, all of the accelerating techniques developed in steady-state problems can be used while marching in this fictitious time. Derivatives with respect to real time t are discretized using a three-point backward-difference formula, which is second-order accurate in time. An explicit four-stage Runge–Kutta scheme is iteratively used in the time integration, and the second-order central-difference method is used for the spatial discretization.

k–ω Model Equations

The dual-time-stepping method is basically implicit. However, it may result in numerical instability of turbulence model equations if an explicit time marching in τ is used because they represent large source terms in the boundary layer. Thus, in the present study an implicit time marching in τ is adopted for the k–ω model equations written in the form of Eq. (4) (Ref. 21). They are now reformulated by applying an approximate factorization scheme to the time marching in τ as follows:

$$\left[I + \Delta\tau\frac{\partial}{\partial\xi}\left(\frac{\partial E_c}{\partial Q} - \frac{\partial E_v}{\partial Q}\right)\right]\cdot\left\{I + \Delta\tau\left[\frac{\partial}{\partial\eta}\left(\frac{\partial F_c}{\partial Q} - \frac{\partial F_v}{\partial Q}\right) - \frac{\partial S}{\partial Q} + \frac{3}{2\Delta t}\right]\right\}\cdot\Delta Q = \Delta\tau R^* \tag{5}$$

where R^* and ΔQ are defined as

$$R^* = [-(3Q^k - 4Q^n + Q^{n-1})/2\Delta t + R^k]$$
$$\Delta Q = Q^{k+1} - Q^k \tag{6}$$

with n denoting the physical time stage and k the fictitious time stage. The first-order upwind scheme is used for the convective terms to enhance the stability and the central-differences scheme is used for the diffusive terms. The lower-order differencing of the convective terms does not significantly affect the second-order accuracy of the mean-flow solution. This is probably because the turbulence affects the mean flow only through eddy viscosity. Again, proper evaluation of the source terms is crucial to the stability of the computation because the source terms become very large in the near-wall region, which causes the equations to be very stiff. Thus, in the present study the source terms are treated implicitly and linearized by assuming that ω/k and μ_T are constant. The source-Jacobian matrix of the k–ω model equations is given by

$$\frac{\partial S}{\partial Q} = \begin{bmatrix} -2/3D_{ij} - 2\beta^*\omega & 0 \\ 0 & -2/3\alpha D_{ij} - 2\beta\omega \end{bmatrix} \tag{7}$$

where $D_{ij} = \max[0, (\partial u/\partial x + \partial v/\partial y)]$.

Convergence Acceleration Schemes

To accelerate the convergence of the solution, locally varying time-step, implicit residual smoothing, and multigrid schemes are applied to the Navier–Stokes equations. In particular, the full approximation storage (FAS) multigrid scheme of Jameson[22] and Brandt[23] is used. As a matter of fact, this scheme is also applied to the k–ω model equations, paying attention to the fact that implementation of multigrid scheme to the turbulence model equations has been only very recently introduced.[24,25] The turbulence-production term $\tau_{ij}(\partial u_i/\partial x_j)$ is calculated only in the finest grid and restricted to the coarse grid because of its nonlinearity. The multigrid scheme is not applied in the viscous sublayer region. That is, the calculation is performed there, but the corrections to the finer grid solution are not because ω varies rapidly from 10^9 to 10^4 in the near-wall region. This steep change can deteriorate the convergence of the solution when there are not sufficient grid points. The source-Jacobian matrix is also used in the coarse grid to reduce the numerical stiffness.

Artificial Dissipation

For the Navier–Stokes equations an eigenvalue scaling of artificial-dissipation terms of fourth-order and second-order differences are included with appropriate scaling in the near-wall region to eliminate odd-even point decoupling and oscillations near the shock waves and stagnation points.[26] A similar type of artificial-dissipation formulation may be used for the k–ω model equations. But we adopt an upwind scheme for the k–ω model equations because of its simplicity and stability.[21]

Boundary Conditions

Because the cell-centered finite volume approach is used, phantom cells are placed outside the boundaries, to which boundary conditions are assigned.

According to the theory of characteristics, three quantities are specified at the subsonic inlet boundary. Freestream values of k and ω are specified according to Menter.[27] At a subsonic outlet the average static pressure is given, while other variables are extrapolated from the interior of the computational domain. At solid surfaces velocity and turbulent kinetic energy are set to zero, and pressure is extrapolated from the interior, while the solid walls are assumed to be adiabatic. The specific dissipation rate ω is specified at the first grid point from the wall as

$$\omega = 6\nu_w \Big/ \tfrac{3}{40}y^2 \quad \text{as} \quad y \to 0 \tag{8}$$

For calculating the rotor-stator interaction we consider that stator and rotor grids have a common interface boundary and the match is imposed through appropriate evaluation of phantom cell values. At the interface boundary the phantom cells of the stator and rotor grids lie inevitably on the adjacent blade passages, respectively. Because O-type grids are to be used, the cell shapes are irregular near the interface boundary. Thus, a bilinear interpolation using the triangle-area method is adopted. This interpolation method may not guarantee the conservations of mass, momentum, and energy across the interface. But accuracy can be retained in an engineering sense when there is not a steep gradient of a flow variable such as a shock wave.

For the steady averaging-plane method the nonreflecting scheme of Chima[3] is applied to the interface of the blade rows. This scheme allows close spacing between blade rows without reflection of flow variables.

Results and Discussion

Flow Around a Bicircular-Arc Airfoil

Experiments on the flow around an 18% thick airfoil were conducted in a wind tunnel at NASA Ames Research Center.[16–18] It was reported that for freestream Mach numbers between 0.74 and 0.78 the flow was unsteady but periodic, with shock-induced separation alternating from one side of the airfoil to the other. The reduced frequency ($=\pi f C/u_\infty$, where C denotes chord length) of the experiment was about 0.49. As the freestream Mach number was increased, it was shown that the shock moved downstream. For Mach numbers higher than 0.78, the flow was steady, and separation occurred on both sides of the airfoil trailing edge.

The present computation is mainly performed at $M=0.76$ and $Re=11\times10^6$. Figure 1 shows the computational grid consisting of two 161×65 grid blocks, where the tunnel walls are contoured according to the data of McDevitt et al.[16] The average value of y^+, the dimensionless distance of the first grid point from the wall, is smaller than unity. In the multigrid calculations three grid levels are adopted, which requires about 50 iterations per cycle for achieving a residual drop of 10^{-6}. The time step was chosen to be $\frac{1}{145}$ of one cycle. This corresponds to the Courant–Friedrichs–Lewy (CFL) number between 2 (outer stream) and 16,000 (boundary layer). The CFL number is maximum at the trailing edge close to the wall because the velocity is rather high because of shock-induced separation and the grid size is very small.

Instantaneous Mach number contours are presented in Fig. 2. A strong separation develops behind a shock wave on the upper side, and it is clear that this separation induces an unsteady motion (Figs. 2a–2c). As explained in Seegmiller et al.,[17] the probable process that initiates the unsteady flowfield depends on two conditions: a slight asymmetry in the location of the separation points on the upper and lower surfaces caused by an inherent code asymmetry and rapid development of a separation zone on one side of the airfoil. The resulting asymmetry in the wake tends to extract mass from the trailing-edge separated region on the other side of the airfoil, as shown in Fig. 3, where instantaneous Mach number contours and streamlines are presented. This extraction of mass causes the flow on the lower side to accelerate so that a shock wave starts to develop (Figs. 2d and 2e). Then, the strength of the shock on the upper side begins to decrease as it advances upstream where local velocities are low (Figs. 2e and 2f). Eventually, it vanishes at about $x/C\approx0.65$, and the separation region collapses to complete one cycle (Fig. 2g). Meanwhile, an identical process is occurring on the lower side 180 deg out of phase. The correct prediction of the size of separation bubble is crucial to a time-accurate calculation.

The time histories and reduced frequencies of pressure fluctuations at two points on the airfoil surface are to be compared with the experimental results of Seegmiller et al.[17] as well as the computational results of Arnone et al.[20] First, we are interested in comparing only the magnitude of pressure fluctuations. Therefore, in Fig. 4 each set of data is represented in terms of time divided by the corresponding period of pressure fluctuations. All of the data correspond to the condition at $M=0.76$ and $Re=11\times10^6$, except that the computational results of Arnone et al. correspond to the condition at $M=0.765$ and $Re=8\times10^6$. At $x/C=0.5$ their data show rather smooth rise and fall of the pressure fluctuation and underestimate it substantially, whereas at $x/C=0.775$ their data slightly underpredict it. This means that their calculated shock was not strong enough because the algebraic turbulence model predicted a small separation behind the shock wave, thus hindering the shock wave from advancing sufficiently far upstream. On the other hand, the present results agree well with the experimental data at $x/C=0.5$, but overpredict the pressure fluctuation by 15% at $x/C=0.775$. This is thought to

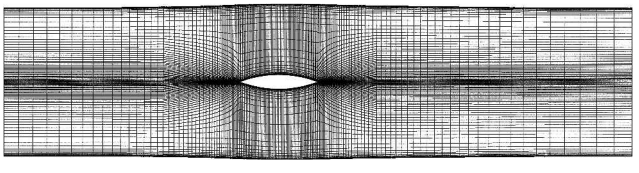

Fig. 1 Two 161×65 H-type grid blocks for calculating the shock buffeting flow.

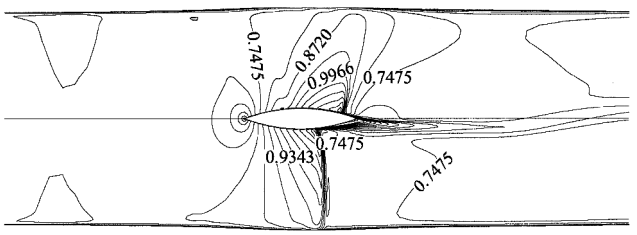

a) Time = $\frac{0}{7}T$

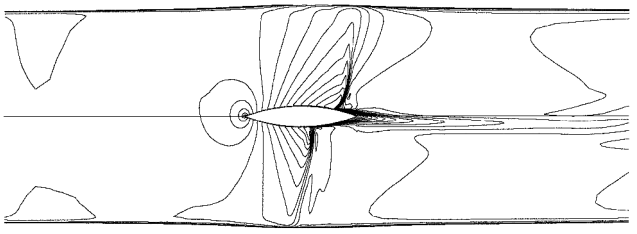

b) Time = $\frac{1}{7}T$

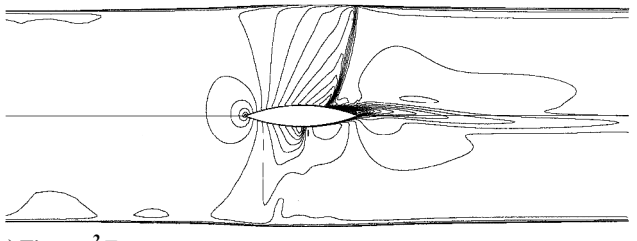

c) Time = $\frac{2}{7}T$

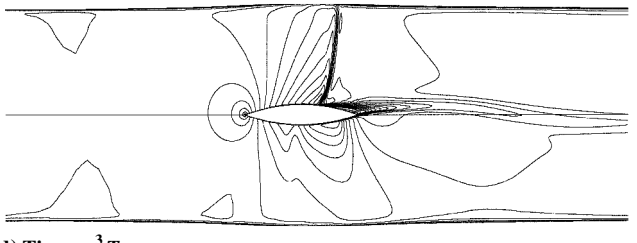

d) Time = $\frac{3}{7}T$

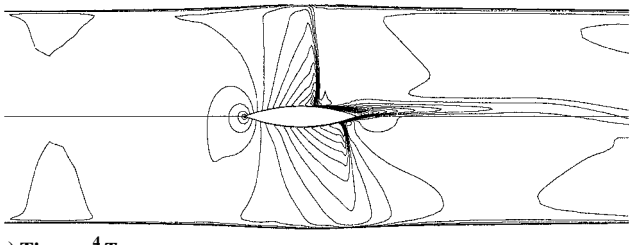

e) Time = $\frac{4}{7}T$

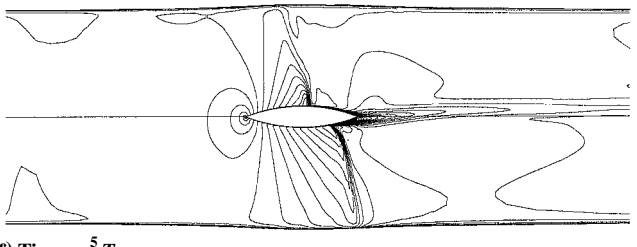

f) Time = $\frac{5}{7}T$

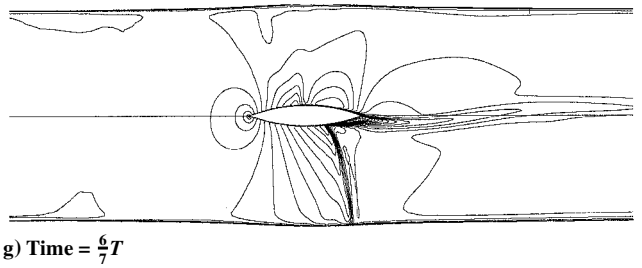

g) Time = $\frac{6}{7}T$

Fig. 2 Instantaneous Mach-number contours for the shock buffeting flow at $M=0.76$.

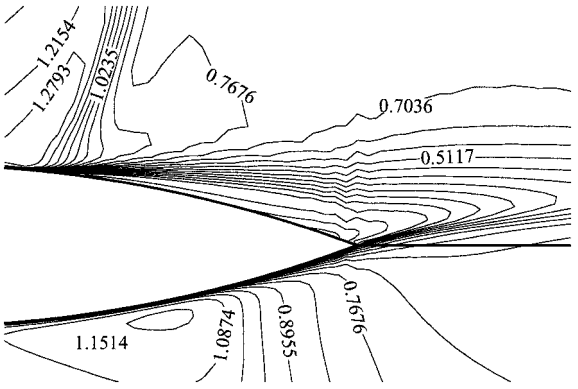

a) Mach-number contours

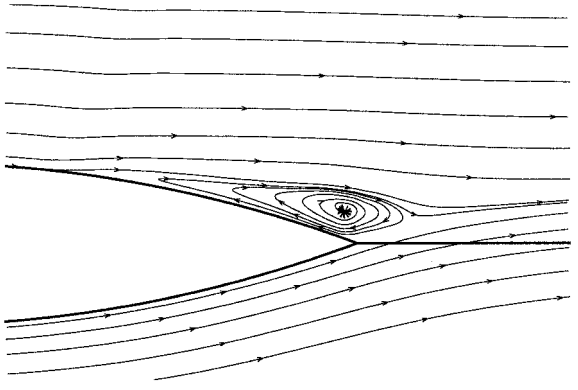

b) Streamlines

Fig. 3 Close-up view of Fig. 2d showing a large separated region at the trailing edge.

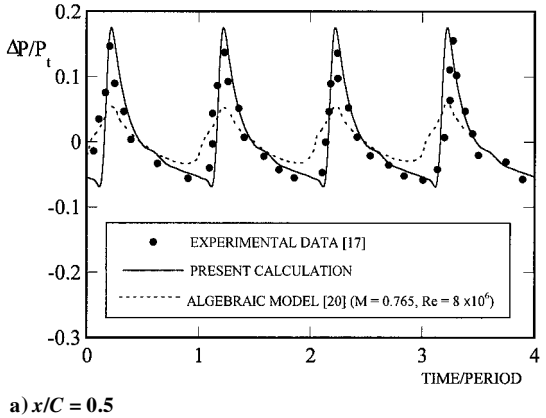

a) $x/C = 0.5$

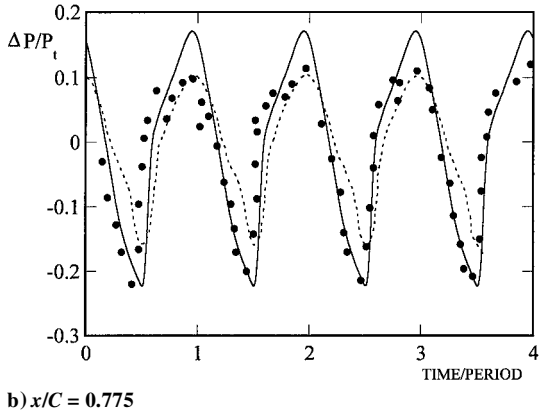

b) $x/C = 0.775$

Fig. 4 Surface-pressure evolutions at two points on the bicircular arc airfoil, $M = 0.76$ and $Re = 11 \times 10^6$.

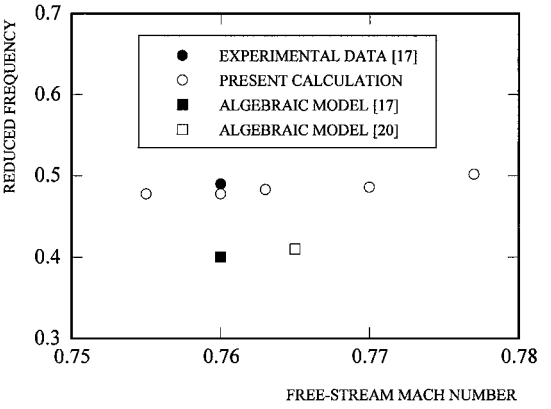

Fig. 5 Reduced frequency vs freestream Mach number.

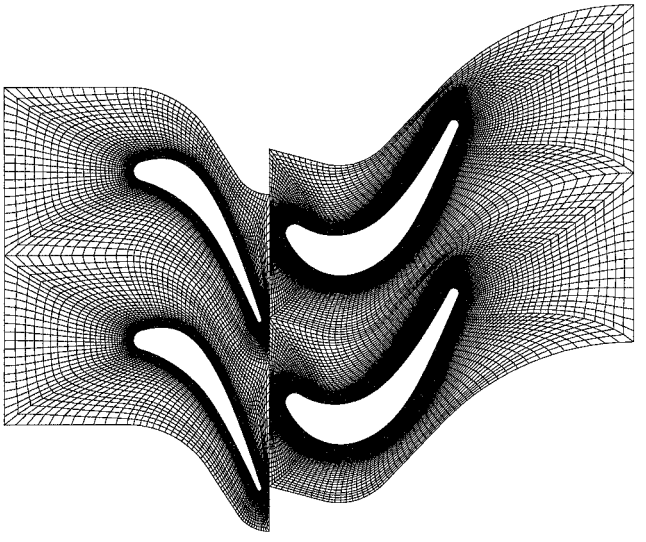

Fig. 6 Two 201 × 69 O-type computational grids for the LSRR turbine stage.

be caused by the stronger intensity of the shock wave in the present prediction than in the experiment.

Next, Fig. 5 shows that the present calculation indicates a reduced frequency of 0.478, which agrees reasonably well with the experimental result, whereas other calculations adopting algebraic turbulence models[17,20] underestimated it by 20% (0.41). The underestimation of the reduced frequency with the algebraic models is quite possibly caused by the prediction of a smaller size of the separated region, which induces the unsteady motion as just explained.

Rotor-Stator Interactions

Calculations are performed to consider the rotor-stator interaction of a single-stage axial turbine, using the geometry and test data of the United Technologies large-scale rotating-rig (LSRR) turbine,[28] which consisted of 22 stator blades and 28 rotor blades. In the present study, however, this turbine is modeled using one stator blade and one rotor blade to save the computational power. The rotor geometry is enlarged by a factor of $\frac{28}{22}$ to maintain the same blockage. A 15% axial gap is used between the stator and rotor blade rows in accordance with the experiment. The rotor rotating speed is $\omega_R = u_1/0.78$, where u_1 is the inlet axial velocity. The inlet Mach number is about 0.07, and the freestream Reynolds number is 100,000/in. (39,370/cm). Figure 6 shows the computational grids of stator and rotor, each consisting of two 201 × 69 grid blocks. O-type grids are generated by an elliptic grid generator and then redistributed in the pitchwise direction using a geometric progression method. The average value of y^+ is again about 1. Computations are performed on a CRAY-J90 supercomputer. Among the four methods for analyzing turbomachinery blade-row flows presented in the

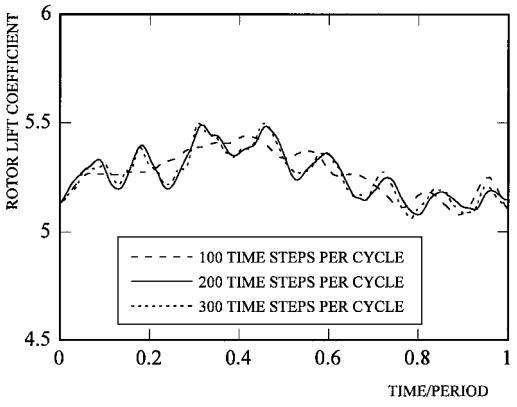

Fig. 7 Evolutions of rotor lift coefficient.

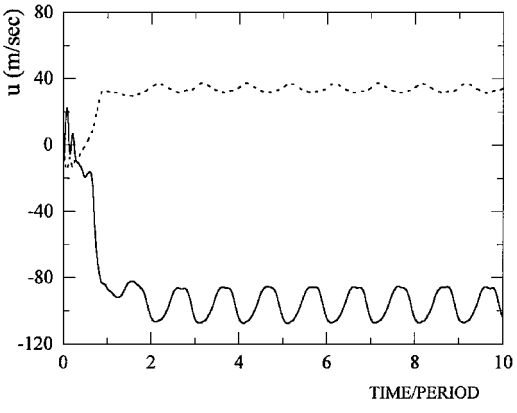

Fig. 8 Time histories of streamwise velocity at two different locations near the rotor leading edge.

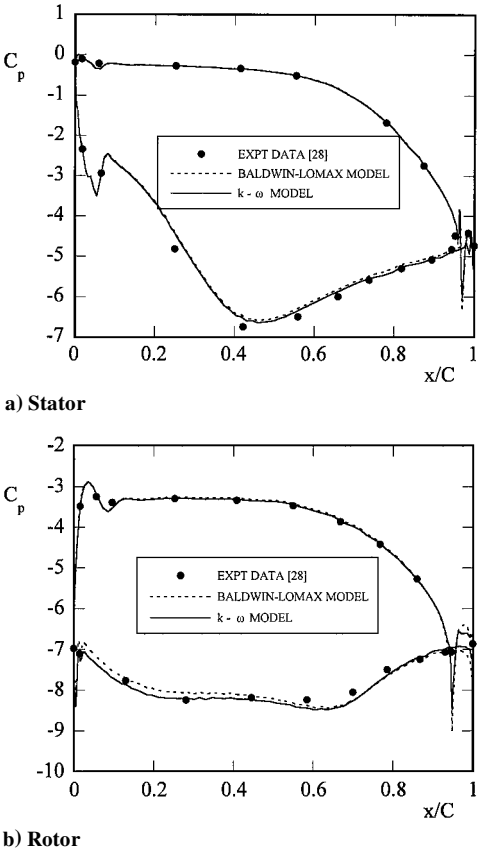

Fig. 9 Time-averaged pressure-coefficient distributions along the stator and rotor blade surfaces.

Introduction, two approaches are applied, namely, the fully unsteady calculation method and the averaging-plane method. Further, computations adopting the Baldwin–Lomax model are also carried out to examine the effect of turbulence models.

Fully Unsteady Calculation

The effect of time-step size on the rotor lift evolution is considered as shown in Fig. 7. It has been confirmed that for a time-step size smaller than $\frac{1}{200}$ of one cycle there are not significant differences in the solution. Thus, a time step of $\frac{1}{200}$ of one cycle is chosen in the present calculation. This corresponds to the CFL numbers between 2 and 7500. Calculations are performed using three grid levels and required about 35 iterations per time step for achieving a residual drop of 10^{-6}. In this case it took about 6180 s per cycle. Because of the close spacing between the stator and rotor blade rows, at the interface boundary the phantom cells of one grid block would be overlaid in the blade passage of the other grid block when the calculation is performed on the coarsest grid. Therefore, at the last stage of convergence only one grid level is adopted. The cost per grid point per iteration ($\Delta\tau$) and the cost per grid point per dual-time step (Δt) are 6.65×10^{-5} s and 2.27×10^{-3} s, respectively. A fully explicit Runge–Kutta computation with a CFL number of 2.5 would have required 3000 iterations per time step, which would take about 3.7×10^5 s per cycle if there were not a stability problem in the calculation of turbulence model equations. Thus, the present method requires $\frac{1}{60}$ of the CPU time of the fully explicit method, which means that the present method can reduce the CPU time by 98%, compared with the fully explicit scheme. Figure 8 describes time histories of streamwise velocity at two different locations near the rotor leading edge. The velocity field becomes time periodic after three or four cycles.

Figure 9 compares the computed time-averaged pressure-coefficient distributions along the stator and rotor blade surfaces with the experimental data of Dring et al.[28] The pressure coefficient is defined as

$$C_p = \frac{P_{\text{avg}} - P_{t1}}{\frac{1}{2}\rho_1 \omega_R^2} \tag{9}$$

where P_{avg} is the average static pressure over one cycle at a given point, P_{t1} the average inlet total pressure, and ρ_1 the average inlet density. The computations using the k–ω model and the Baldwin–Lomax model both agree well with the experimental data except at $x/C = 0.3$ of the stator suction side and at $x/C = 0.65$ of the rotor suction side. These discrepancies are probably caused by the three-dimensional effects caused by the low aspect ratio of the experimental airfoil.[5,6]

The magnitudes of the unsteady pressure along the stator and rotor surfaces are shown in Fig. 10. The unsteady pressure amplitude coefficient is defined as

$$P_a = \frac{P_{\max} - P_{\min}}{\frac{1}{2}\rho_1 \omega_R^2} \tag{10}$$

where $P_{\max}$ and $P_{\min}$ represent the maximum and minimum pressures occurring over one cycle at a given location. In the case of the stator, the agreement between calculation and experiment is fairly good despite the fact that the rotor geometry is scaled up, whereas, in the case of the rotor, the pressure fluctuation is somewhat overpredicted near the trailing edge. This trend is consistent with previous results,[2,5] and an improvement can be made by a combination of including three-dimensionality and multipassage approach.[7] The Baldwin–Lomax model shows a similar trend to the k–ω model except that it predicts somewhat smaller values than the latter. However, the differences between the results of the two models are not so significant as those for the shock buffeting case. The effect of turbulence models on the rotor-stator interaction may not be substantial as long as the extent of the separated region involved is small and the flow is largely inviscid. Thus, in the remaining part of the present paper, only the computational results obtained by the k–ω

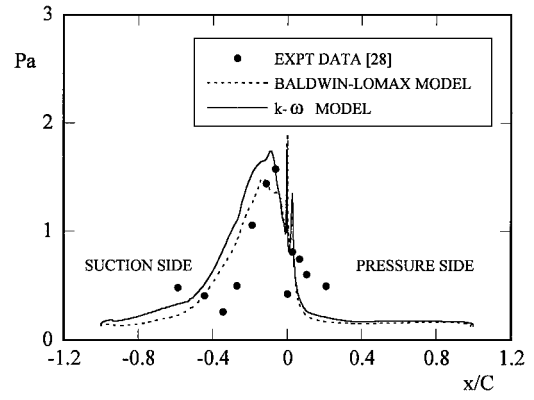

a) Stator

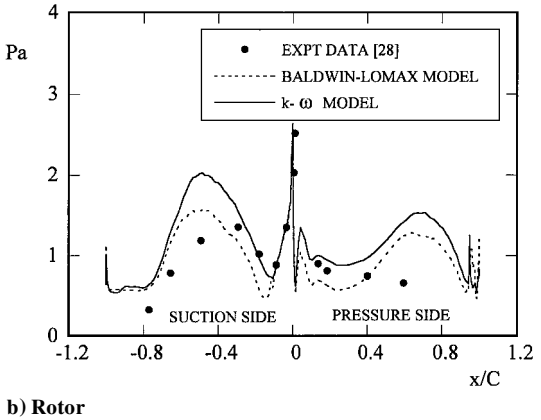

b) Rotor

Fig. 10 Pressure amplitude coefficients.

model are presented, wherever discussions are made in connection with turbulence characteristics of the flowfield.

Figure 11 depicts instantaneous Mach-number contours during one blade-passing cycle, in which two types of interactions are salient, i.e., potential-flow and wake interactions. As the rotor blade moves down (Figs. 11a–11c), the Mach-number contours of the stator blade passage, particularly at the suction side, vary in the fashion of potential-flow interaction. The presence of the rotor influences the flowfield around the stator. When the rotor comes close to the stator (Figs. 11d and 11a), the Mach number increases near the stator trailing edge. Then it is clearly seen that the wake convected from the stator trailing edge collides with the rotor leading edge, which manifests the wake interaction between the stator and rotor. On the other hand, in Figs. 11a and 11b where the wake goes from a fine grid region to the coarse corner of the next grid, the wake widens quickly across the interface boundary. Therefore, the accuracy of simulating the wake convection may be affected, so that H-type grids or H-type overlaid grids embedded with O-type grids are recommended to be used to improve this situation.[2,5,8]

The wake-interaction mechanism is more evident in Fig. 12, which shows instantaneous turbulent kinetic energy contours corresponding to turbulent intensities greater than about 2% and skin-friction coefficient distributions along the rotor blade surface during one cycle. The skin-friction coefficient is defined as

$$C_f = \tau_w \Big/ \tfrac{1}{2}\rho\omega_R^2 \tag{11}$$

The turbulent kinetic energy level at the rotor boundary layer becomes high when the stator wake collides with the rotor leading edge, as shown in Fig. 12a. The boundary layer remains laminar along the pressure surface ($S/C > 0$), but it undergoes transition and becomes turbulent along the suction surface ($S/C < 0$), where S denotes arc distance along the blade surface. The small rise and fall of C_f at $-0.4 < S/C < -0.1$ are considered to be caused by to the curvature effect, which can be seen in Fig. 11 as a bubble-like shape near the leading edge of the suction side of the rotor blade. Then, the

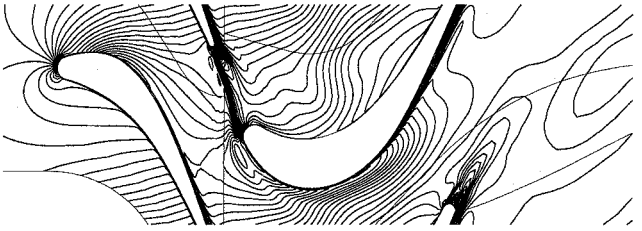

a) Time = $\frac{0}{4}T$

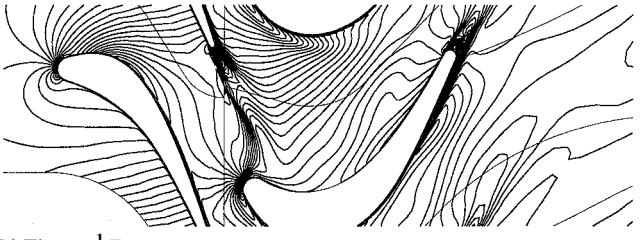

b) Time = $\frac{1}{4}T$

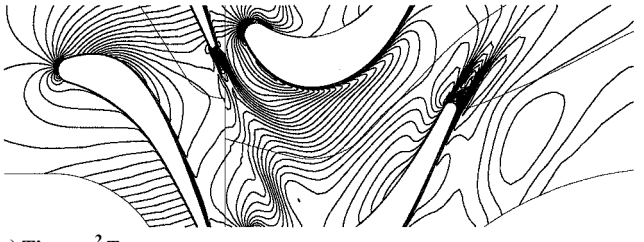

c) Time = $\frac{2}{4}T$

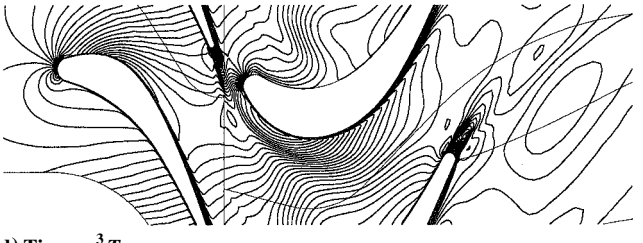

d) Time = $\frac{3}{4}T$

Fig. 11 Instantaneous Mach-number contours during one blade-passing cycle.

boundary layer undergoes transition at $S/C \approx -0.5$ and becomes turbulent. As the rotor blade moves down, the transition point is shown to occur farther downstream in Fig. 12b than in Fig. 12a. Consequently, Fig. 12c shows the existence of laminar-like flow regime on the suction side because the wake effect is confined to the pressure side. When the rotor blade is close to the wake prior to colliding, skin friction becomes high because of the boundary-layer thinning caused by the high-pressure region in the wake (potential-flow effect). The boundary layer is further thinned, and skin friction becomes higher in Fig. 12e. Maximum skin friction occurs when the wake collides with the leading edge of the rotor blade, which triggers flow transition from laminar to turbulent. This is possibly because of the high level of kinetic energy in the wake region.

Steady Calculation

The convergence of the calculation can be greatly enhanced by using the multigrid method when the inviscid flowfield develops. However, after the development of the inviscid flowfield, the viscous flowfield develops, and the use of multigrid does not enhance the convergence any more. Thus, in the present study one grid level is adopted at the last stage of convergence. A multigrid algorithm employing three grid levels is used until a residual drop of 10^{-5} is achieved, and then one grid level is used for a residual drop of 10^{-6}, which requires about 4300 time steps and 3600 s, as shown in Fig. 13.

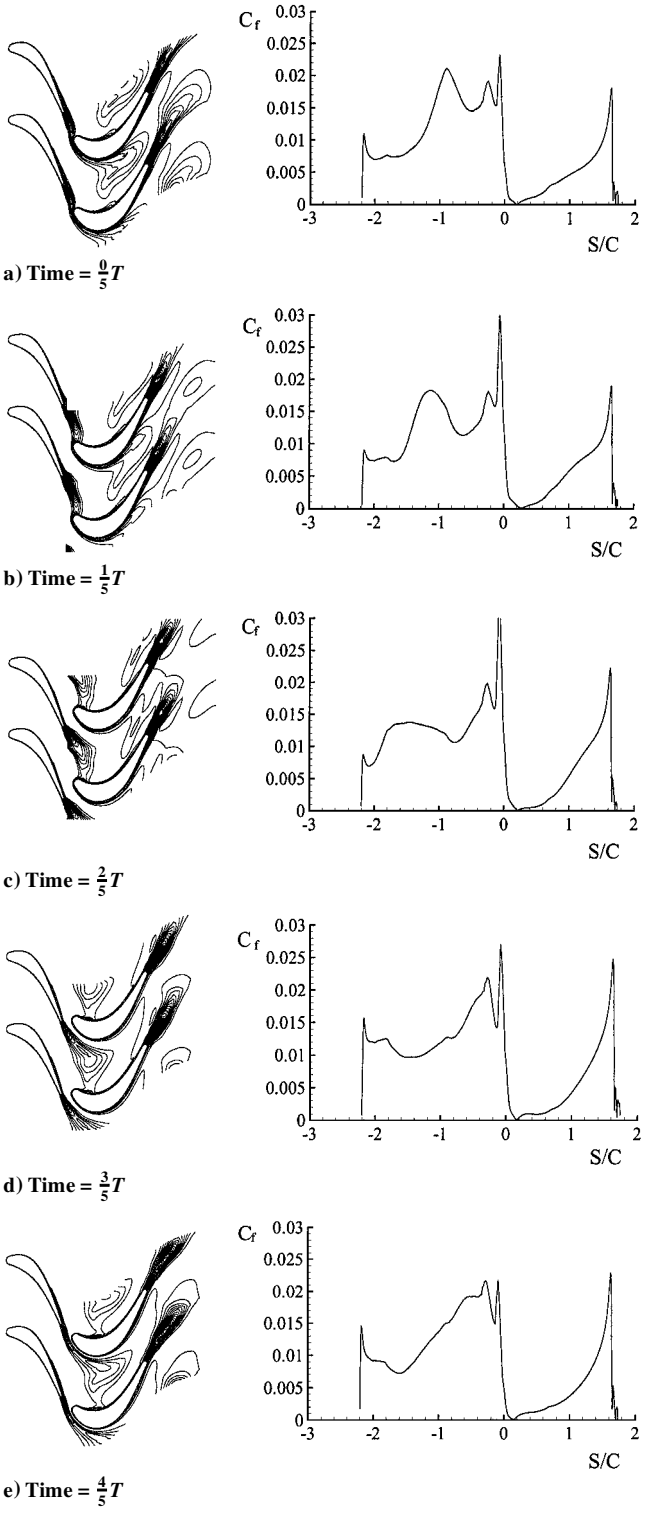

Fig. 12 Instantaneous turbulent kinetic energy contours and skin-friction coefficient distributions along the rotor blade surface during one cycle.

Figure 14 depicts the pressure-coefficient distributions along the stator and rotor blade surfaces, where there are again little differences between the results of the $k-\omega$ model and the Baldwin–Lomax model. Although it is believed that grid-independent solutions are obtained, the pressure-coefficient distributions on the stator suction surface and on the rotor pressure surface show large differences from the experimental data. These discrepancies can be explained by comparing the Mach-number contour plots in Figs. 11 and 15, from which it is noted that the unsteady motion of the rotor influences stator suction side and rotor pressure side more than other

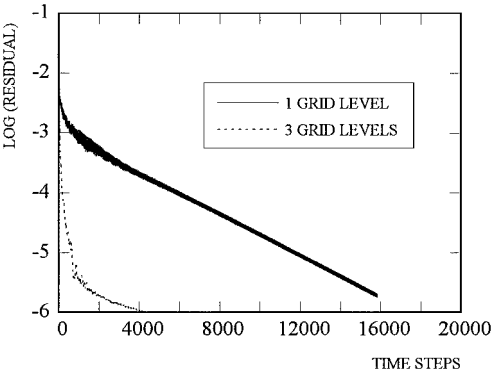

Fig. 13 Convergence histories of the steady calculation.

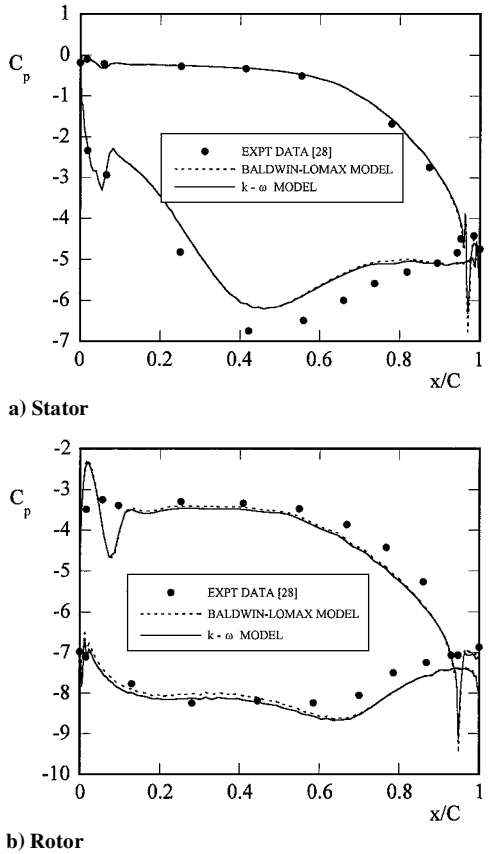

Fig. 14 Pressure-coefficient distributions along the stator and rotor blade surfaces.

sides. Then, it is clear that the steady approach predicts pretty well the steady-like portions of the unsteady motions. Kinetic energy contours are also shown in Fig. 15c, which are smooth without any wiggles on both sides of the interface boundary, indicating that the nonreflecting boundary conditions are successfully implemented. However, it is noteworthy that the convection of turbulent kinetic energy through wake effects is lacking here because mixed-out average is used at the interface.

Figure 16 shows the skin-friction coefficient distributions along the rotor blade surface obtained by both methods. In comparison with the unsteady calculation, the steady calculation shows a somewhat higher level of skin-friction distribution, but qualitatively there is no significant difference between the results of unsteady and steady calculations. The skin-friction distributions along the stator blade surface are not presented here for brevity because very little is worthy of discussion.

We argue that algebraic turbulence models and the steady approaches may predict the potential-flow properties well with small

Table 1 Comparison between unsteady and steady calculations

Parameter	Unsteady calculation			Steady calculation			Experimental conditions
	$k-\omega$ model: present study	Baldwin–Lomax model		$k-\omega$ model: present study	Baldwin–Lomax model		
		Present study	Ref. 2		Present study	Ref. 2	Ref. 28
Absolute flow angle at the stator exit	−68.55 deg	−67.46 deg	−66.89 deg	−68.36 deg	−68.17 deg	−67.7 deg	−67.5 deg
Relative flow angle at the rotor inlet	−48.76 deg	−48.28 deg	−47.66 deg	−49.76 deg	−49.38 deg	−47.27 deg	−50 deg
Relative flow angle at the rotor exit	64.11 deg	64.02 deg	63.15 deg	64.60 deg	64.28 deg	63.3 deg	64.5 deg
CPU time	6180 s/cycle	5510 s/cycle	——	3600 s	2909 s	——	——

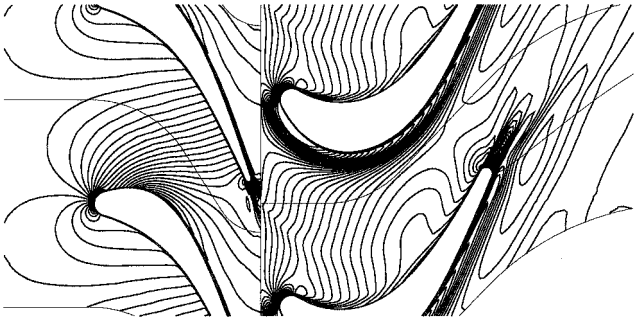

a) Mach number

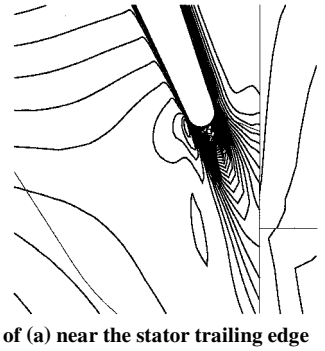

b) Close-up view of (a) near the stator trailing edge

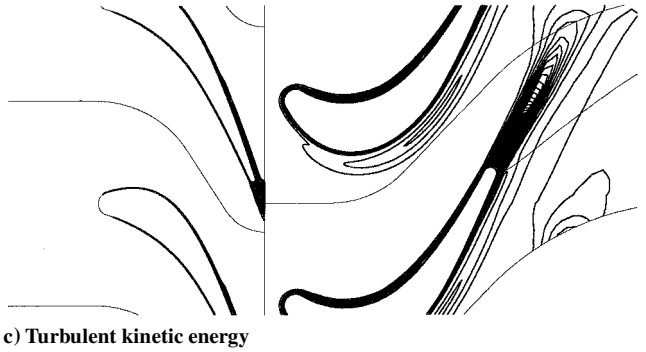

c) Turbulent kinetic energy

Fig. 15 Contour plots for the steady calculation.

CPU time requirements, but they cannot properly describe the convection of the turbulent kinetic energy downstream of the stator, which has significant effects on the boundary-layer transition and heat transfer over the rotor blade surface. This kind of transition is called wake-induced transition and mainly affected by the turbulence of the upstream wakes, rather than by the level of the velocity defect.[29,30] For these situations two-equation turbulence models and unsteady approaches are more adequate, by which the convection of turbulent kinetic energy is better simulated without prescribing the transition point beforehand. Although the present $k-\omega$ model cannot predict properly the onset of transition over the turbine blade surface under the presence of stagnation points and, further, cannot predict wake-induced transition precisely, we believe that it can still represent the general trend of the transition. For future study it is highly desirable to incorporate an accurate transition model.

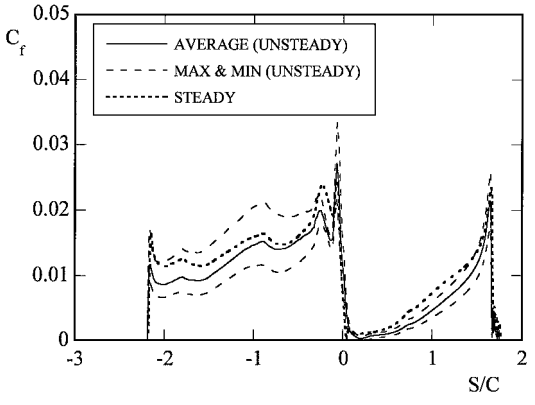

Fig. 16 Skin-friction coefficient distributions along the rotor blade surface.

Table 1 shows a comparison of the time-averaged flow angles and CPU times between the unsteady and steady methods. The flow angles obtained by the present calculations are generally in better agreement with the nominal operating conditions[28] than those obtained by previous calculations.[2] Incidentally, the relative flow angles at the rotor inlet and outlet obtained by the present steady calculation using the $k-\omega$ model are in excellent agreement with the given conditions. The unsteady method adopting the $k-\omega$ model requires 6200 s per cycle and a total of about 24,000 s including the CPU time to obtain time-periodic solutions. Overall, the unsteady approach requires seven times the CPU time of the steady approach. Calculations adopting the Baldwin–Lomax model show similar results with about 10 ~ 20% reduction of the CPU time, which is caused by the fact that it does not need to solve extra two transport equations.

Conclusions

Compressible unsteady flows past a bicircular arc airfoil and through the LSRR turbine blade rows are calculated mainly by using a low-Reynolds-number $k-\omega$ turbulence model. An explicit four-stage Runge–Kutta solver for the Navier–Stokes equations and an implicit approximate factorization scheme for the $k-\omega$ model equations are proposed in connection with the use of dual-time-stepping and multigrid schemes. Much CPU time can be saved by adopting this hybrid method.

The low-Reynolds-number $k-\omega$ turbulence model has been successfully applied to the shock buffeting phenomena over a bicircular-arc airfoil, providing good agreements with the experiment in terms of shock-wave boundary-layer interaction and the related separation phenomena. In regard to this, it is discussed that a close prediction of the size of the separation bubble behind a shock wave plays an important role, which is better embodied by the $k-\omega$ model than by the algebraic turbulence model.

When we applied the present method to the fully unsteady calculation of the rotor-stator interaction in a turbine stage, we again obtained a satisfactory agreement with the experiment in terms of pressure-coefficient distributions and flow angles. For this case it is

discussed that the effect of turbulence models is not so substantial because of the existence of small separated regions. The steady averaging-plane method also showed fairly good overall performance. However, it is emphasized that wake effects must be included in the computational investigation to account for the turbulence characteristics of the flowfield because the convection of the turbulent kinetic energy may affect the rotor performance by triggering an early transition from laminar to turbulent flows.

Acknowledgment

This work was supported by the Turbo and Power Machinery Research Center, Seoul National University, Korea and System Engineering Research Institute, Taejon, Korea.

References

[1]Dorney, D. J., and Sharma, O. P., "Evaluation of Flow Field Approximations for Transonic Compressor Stages," *Journal of Turbomachinery*, Vol. 119, No. 3, 1997, pp. 445–451.

[2]Dorney, D. J., Davis, R. L., and Sharma, O. P., "Unsteady Multistage Analysis Using a Loosely Coupled Blade Row Approach," *Journal of Propulsion and Power*, Vol. 12, No. 2, 1996, pp. 274–282.

[3]Chima, R. V., "Calculation of Multistage Turbomachinery Using Steady Characteristic Boundary Conditions," AIAA Paper 98-0968, Jan. 1998.

[4]Chima, R. V., "Explicit Multigrid Algorithm for Quasi-Three-Dimensional Viscous Flows in Turbomachinery," *Journal of Propulsion and Power*, Vol. 3, No. 5, 1987, pp. 397–405.

[5]Rai, M. M., "Navier–Stokes Simulations of Rotor-Stator Interactions Using Patched and Overlaid Grids," *Journal of Propulsion and Power*, Vol. 3, No. 5, 1987, pp. 387–396.

[6]Rai, M. M., "Three-Dimensional Navier–Stokes Simulations of Turbine Rotor-Stator Interaction," *Journal of Propulsion and Power*, Vol. 5, No. 3, 1989, pp. 307–319.

[7]Madavan, N. K., Rai, M. M., and Gavali, S., "Multipassage Three-Dimensional Navier–Stokes Simulation of Turbine Rotor-Stator Interaction," *Journal of Propulsion and Power*, Vol. 9, No. 3, 1993, pp. 389–396.

[8]Arnone, A., Pacciani, R., and Sestini, A., "Multigrid Computations of Unsteady Rotor-Stator Interaction Using the Navier–Stokes Equations," *Journal of Fluids Engineering*, Vol. 117, No. 4, 1995, pp. 647–652.

[9]Dorney, D. J., "Reynolds-Averaged Navier–Stokes Studies of Low Reynolds Number Effects on the Losses in a Low Pressure Turbine," NASA CR 198534, Sept. 1996.

[10]Dorney, D. J., and Ashpis, D. E., "Study of Low Reynolds Number Effects on the Losses in Low-Pressure Turbine Blade Rows," AIAA Paper 98-3575, July 1998.

[11]Hah, C., Puterbaugh, S. L., and Copenhaver, W. W., "Unsteady Aerodynamic Flow Phenomena in a Transonic Compressor Stage," *Journal of Propulsion and Power*, Vol. 13, No. 3, 1997, pp. 329–333.

[12]Dorney, D. J., Sharma, O. P., and Gundy-Burlet, K. L., "Physics of Airfoil Clocking in a High-Speed Axial Compressor," American Society of Mechanical Engineers, Paper 98-GT-082, June 1998.

[13]Chien, K. Y., "Prediction of Channel and Boundary-Layer Flows with a Low Reynolds Number Turbulence Model," *AIAA Journal*, Vol. 20, No. 1, 1982, pp. 33–38.

[14]Wilcox, D. C., "A Half Century Historical Review of the k–ω Model," AIAA Paper 91-0615, Jan. 1991.

[15]Menter, F. R., "Improved Two-Equation k–ω Turbulence Models for Aerodynamic Flows," NASA TM-103975, 1992.

[16]McDevitt, J. B., Levy, L. L., Jr., and Deiwert, G. S., "Transonic Flow About a Thick Circular-Arc Airfoil," *AIAA Journal*, Vol. 14, No. 5, 1976, pp. 606–613.

[17]Seegmiller, H. L., Marvin, J. G., and Levy, L. L., Jr., "Steady and Unsteady Transonic Flow," *AIAA Journal*, Vol. 16, No. 12, 1978, pp. 1262–1270.

[18]Levy, L. L., Jr., "Experimental and Computational Steady and Unsteady Transonic Flows About a Thick Airfoil," *AIAA Journal*, Vol. 16, No. 6, 1978, pp. 564–572.

[19]Jameson, A., "Time Dependent Calculations Using Multigrid, with Applications to Unsteady Flows Past Airfoils and Wings," AIAA Paper 91-1596, June 1991.

[20]Arnone, A., Liou, M.-S., and Povinelli, L. A., "Integration of Navier–Stokes Equations Using Dual Time Stepping and a Multigrid Method," *AIAA Journal*, Vol. 33, No. 6, 1995, pp. 985–990.

[21]Choi, C. H., and Yoo, J. Y., "Cascade Flow Calculations Using the k–ω Turbulence Model with Explicit-Implicit Solver," *AIAA Journal*, Vol. 35, No. 9, 1997, pp. 1551, 1552.

[22]Jameson, A., "Transonic Flow Calculations," Mechanical and Aerospace Engineering Dept., Princeton Univ., MAE Rept. 1651, Princeton, NJ, July 1983.

[23]Brandt, A., "Multi-Level Adaptive Computations in Fluid Dynamics," AIAA Paper 79-1455, July 1979.

[24]Zheng, X., Liao, C., Liu, C., Sung, C. H., and Huang, T. T., "Multigrid Computation of Incompressible Flows Using Two-Equation Turbulence Models: Part I—Numerical Method," *Journal of Fluids Engineering*, Vol. 119, No. 4, 1997, pp. 893–899.

[25]Gerlinger, P., and Bruggemann, D., "An Implicit Multigrid Scheme for the Compressible Navier–Stokes Equations with Low-Reynolds-Number Turbulence Closure," *Journal of Fluids Engineering*, Vol. 120, No. 2, 1998, pp. 257–262.

[26]Martinelli, L., "Calculations of Viscous Flows with a Multigrid Method," Ph.D. Dissertation, Mechanical and Aerospace Engineering Dept., Princeton Univ., Princeton, NJ, Oct. 1987.

[27]Menter, F. R., "Influence of Freestream Values on k–ω Turbulence Model Predictions," *AIAA Journal*, Vol. 30, No. 6, 1992, pp. 1657–1659.

[28]Dring, R. P., Joslyn, H. D., Hardin, L. W., and Wagner, J. H., "Turbine Rotor-Stator Interaction," *Journal of Engineering for Power*, Vol. 104, No. 4, 1982, pp. 729–742.

[29]Halstead, D. E., Wisler, D. C., Okiishi, T. H., Walker, G. J., Hodson, H. P., and Shin, H.-W., "Boundary Layer Development in Axial Compressors and Turbines Part 1 of 4: Composite Picture," American Society of Mechanical Engineers, Paper 95-GT-461, June 1995.

[30]Orth, U., "Unsteady Boundary-Layer Transition in Flow Periodically Disturbed by Wakes," *Journal of Turbomachinery*, Vol. 115, No. 4, 1993, pp. 707–713.